



OXFORD CENTRE FOR COLLABORATIVE APPLIED MATHEMATICS

Report Number 11/03

Spontaneous rotational inversion in *Phycomyces*

by

Alain Goriely and Michael Tabor



Oxford Centre for Collaborative Applied Mathematics
Mathematical Institute
24 - 29 St Giles'
Oxford
OX1 3LB
England

Spontaneous rotational inversion in *Phycomyces*

Alain Goriely

OCCAM, Mathematical Institute, University of Oxford

Michael Tabor

Program in Applied Mathematics, University of Arizona, AZ 85721

The filamentary fungus *Phycomyces blakesleeanus* undergoes a series of remarkable transitions during aerial growth. During what is known as the Stage IV growth phase, the fungus extends while rotating in a counterclockwise manner when viewed from above (Stage IVa) and then, while continuing to grow, spontaneously reverses to a clockwise rotation (Stage IVb). This phase lasts for 24 - 48 hours and is sometimes followed by yet another reversal (Stage IVc) before the overall growth ends. Here, we propose a continuum mechanical model of this entire process using nonlinear, anisotropic, elasticity and show how helical anisotropy associated with the cell wall structure can induce spontaneous rotation and, under appropriate circumstances, the observed reversal of rotational handedness.

PACS numbers: 46.70.Hg,87.10.Pq,87.19.lx

Phycomyces blakesleeanus is the most studied phycomyces, a genus of fungi first reported in the early nineteenth century and described at length by the Belgian biologist and cleric Jean-Baptiste Carnoy in 1870 [1]. After a complex reproductive cycle this fungus emerges out of the mycelium as a strikingly large, single-celled, aerial hypha – known as the sporangiophore – reaching sizes of up to 10cm long (See Fig. 1). The organism, its rotating growth phases, and remarkable tropic responses to various external stimuli has long been a source of fascination to biologists and biophysicists alike [2].

Helical growth is the rotation of a structure as it extends axially and is observed in many different tubular structures across the plant kingdom [3]. However, it is not known whether this type of growth serves a biological function or provides some mechanical advantage (as hypothesized in the spiral grain of trees [4]). Nevertheless, elucidating the physical processes that lead to helical growth provides insights into the fundamental problem of relating cell wall structure to growth and form in plants. The physical explanation for helical growth is based on the intuitive notion that a cylinder with a helically structured (cell) wall, under axial stress due to turgor pressure, should unwind in the absence of an external axial moment. Hence, helical growth can be viewed as the macroscopic mechanical consequence of cell wall anisotropy. To set the terminology, we refer to right-handed growth (RH) when a point on top of the cylinder, viewed from above, turns counter-clockwise during extension, and left-handed growth (LH) when the same point turns clockwise.

Similar to other systems exhibiting helical growth, the cell wall of the cylindrically structured sporangiophore of *Phycomyces blakesleeanus* is anisotropic, essentially composed of chitin microfibrils embedded in an elastic matrix of amorphous material made out of chitosan and chitin [5]. After an initial aerial growth phase (Stage I) and the

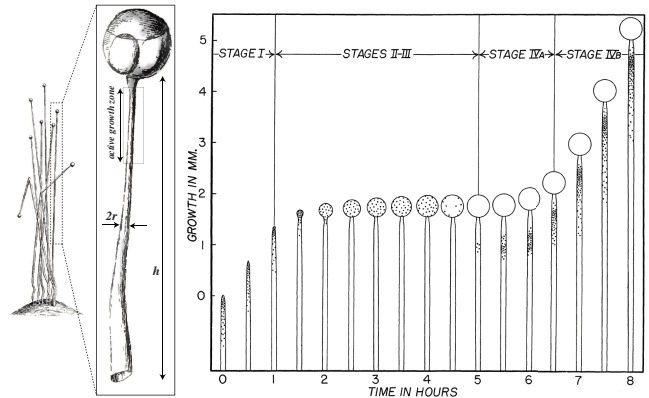


FIG. 1: Left: The fungus *Phycomyces blakesleeanus* as drawn by Carnoy [1]. The spherical dome on top of the tube is the sporangium that contains the spores that are disseminated on completion of the life cycle. Right: The 4 stages of growth for the aerial hypha. In Stage IV helical growth reversal is observed: Stage IVa exhibits right-handed growth and Stage IVb presents left-handed growth. Stage IVb continues for up to 2 days when the organisms can reach up to 10cm in height (reproduced from [6]).

development of the sporangium (Stages II and III), axial growth resumes in Stage IV. A remarkable behavior is then observed [6]: in Stage IVa, RH growth takes place for approximately 1 hour; this is followed by Stage IVb in which LH growth is observed that can last up to 48 hours. A further rotational inversion (Stage IVc) has also been reported by some authors [7]. In a series of experimental and theoretical papers, Ortega, Gamow and co-workers have presented a geometric explanation for the rotation in Stage IVb based on the reorientation of the microfibrils during growth [8]. They also suggested that the inversion of rotation may be due to a so-called “microfibril slippage” effect but they did not further elaborate on the mechanics of this process.

Here we present a mechanical model for the rotational reversals observed in Stages IVa, IVb, and IVc. We view the sporangiophore as a growing, fiber-reinforced, elastic structure and include a dynamical remodeling and deposition of the fibers. Our basic assumption is that new fibers are deposited in a stress-free state along the direction of existing fibers. The fiber angle starts close to the horizontal direction in a right-handed orientation and the growth zone increases to its asymptotic size. The rotation of the tube is then simply obtained from the mechanical balance that results from the extension of an anisotropic elastic tube under pressure in the absence of an end moment. Strikingly, the model predicts that under extension a fiber will always tend to align in the axial direction but that the tube can either rotate clockwise or counter-clockwise depending on the angle of the fibers and their state of stress. Within this model, the initial RH growth is shown to be a transient phenomenon that disappears when the growth zone is sufficiently extended. Once the growth zone is fully established, a regular LH growth persists with constant rotation up to a point when the growth zone starts retracting and a further inversion is possible, again as a short transient phenomenon.

The length and time scales in Stages IVa and IVb are as follows. A typical radius of the sporangiophore is $50\mu\text{m}$ and we will use this radius (assumed to be constant throughout these phases) as the characteristic length scale, l . The wall thickness is $0.6\mu\text{m} \sim l/83$. The growth zone, which is the zone immediately below the sporangium where new cell wall material is added, extends to to a size h , where $h \sim 3\text{mm} \sim 60l$. A typical sporangiophore length is $15 - 20 \times 10^4 \mu\text{m} \sim 3 - 4 \times 10^3 l$. The typical axial velocity, v_z , in Stage IVb is a constant 3mm/hr , *i.e.* $v_z = 60l/\text{hr}$, which corresponds to an approximate doubling time of one hour for the size of the growth zone [9]. This is accompanied by an angular rotation in Stage IVb of approximately $4\pi/\text{hr}$ for a duration of 24-48 hours. In contrast, Stage IVa last about 1 hour. A typical internal turgor pressure is about 0.4 MPa [10].

We model the sporangiophore as an anisotropic, elastic, incompressible tube with two family of embedded fibres. The first family of fibres is in the hoop direction and provides the cylinder with sufficiently strong radial reinforcement such that under pressure the radius is constant and expansion is confined to a pure extension along the axis. The second family of fibres winds helically (right-handed [11]) around the axis and induces a rotation of the cylinder under extension. The presence of the hoop fibers together with the relative thinness of the wall compared to the radius are used to justify the modeling assumption that there is no variation (strain or stress) in the radial direction and the that tube radius is constant. Also, since the growth zone is much larger than the radius, we neglect gradient effects in the axial direction.

We consider finite deformations in which the cylinder

is allowed to grow, rotate around its axis, and elongate axially while remaining cylindrical. Thus, in cylindrical coordinates with the z -axis corresponding to the vertical axis of growth, the rotation is $\theta = \Theta + \tau\zeta Z$, where τ is the torsion, and the axial stretch is $\zeta = z/Z$ (here upper case symbols correspond to the reference configuration before pressure is applied). The material response is specified by the standard reinforcing model [12] with the simplest possible dependence for its isotropic and anisotropic parts $W(I_1, I_4) = \mu_1/2(I_1 - 3) + \mu_4/4(I_4 - \nu^2)^2$ where the Cauchy-Green tensor invariants are $I_1 = \zeta^2\tau^2 + \zeta^2 + 1/\zeta^2 + 1$, $I_4 = \zeta \sin \Phi (\zeta (\tau^2 + 1) \sin \Phi) + 2\tau \cos \Phi + \cos^2 \Phi$. The angle Φ denotes the orientation of the fibers with respect to the horizontal plane in the reference configuration and ν is the pre-compression of the fibers in the initial configuration ($\nu > 1$ corresponds to fibers that are compressed). It is straightforward to show that the fiber orientation, ϕ , in the current configuration is

$$\phi = \arctan \left(\frac{\zeta \sin \Phi}{\cos \Phi + \zeta \tau \sin \Phi} \right) \quad (1)$$

where we have assumed a thin-walled cylinder of constant (unit) radius.

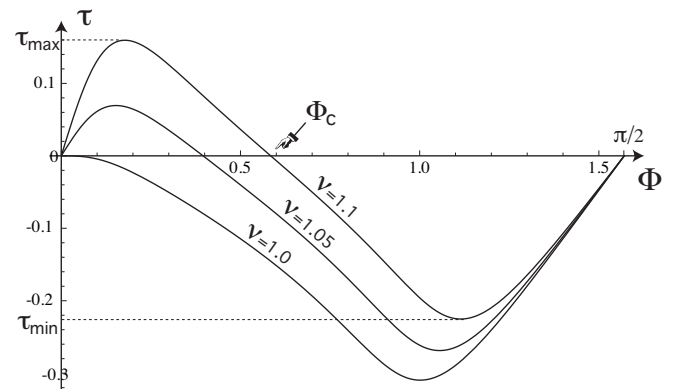


FIG. 2: Effect of fiber pre-compression on torsion τ as a function of the fiber angle Φ ($\mu = 5, \zeta = 1.4$).

We first consider a static model and assume that our tube is uniform with height H and a fixed fiber angle with a right-handed helical configuration $0 < \Phi < \pi/2$. We then subject it to an internal pressure leading to a given extension ζ that we use to parameterize the internal load. From the strain-energy function, we compute the Cauchy stress tensor \mathbf{T} . The only relevant component of \mathbf{T} for our analysis is

$$T_{\theta z} = \mu_1 \zeta^2 \tau + \zeta \mu_4 \sin \Phi (\zeta \tau \sin \Phi + \cos \Phi) \times (\zeta \sin \Phi (\zeta (\tau^2 + 1) \sin \Phi + 2\tau \cos \Phi) + \cos^2 \Phi - \nu^2).$$

Since no axial moment is applied on the surface of the tube, the condition $T_{\theta z} = 0$ leads to a cubic equation for τ for given values of Φ , ν , ζ and ratio $\mu = \mu_4/\mu_1$. This

is the torsion needed to relax the torsional stress in the tube induced by the anisotropy. Some of these solutions are shown in Fig 2.

In the absence of pre-compressed fibers ($\nu = 1$) we see that the twist τ is always negative, *i.e.* the top of tube will rotate clockwise by an angle $\Theta = \tau h = \tau \zeta H$ leading to the appearance of left-handed growth. The effect of pre-compression in the fibers is quite remarkable and non-intuitive. Even for small levels of pre-compression (*e.g.* $\nu = 1.05$), at small fiber angles, the cylinder will rotate counter-clockwise as shown in Fig. 2. The critical fiber angle Φ_c at which there is no rotation is given by $\Phi_c = \arccos\left(\sqrt{(\zeta^2 - \nu^2)/(\zeta^2 - 1)}\right)$ and clearly requires $\zeta > \nu$. The inversion occurs when fibers go from compression to tension, since the critical angle corresponds to the point $I_4 = \nu^2$. In the absence of pre-compression, the cylinder rotates clockwise. Despite the torsional inversion, the fiber orientation in the current configuration is always greater than the orientation in the reference configuration. This is illustrated in Fig 3. From the ex-

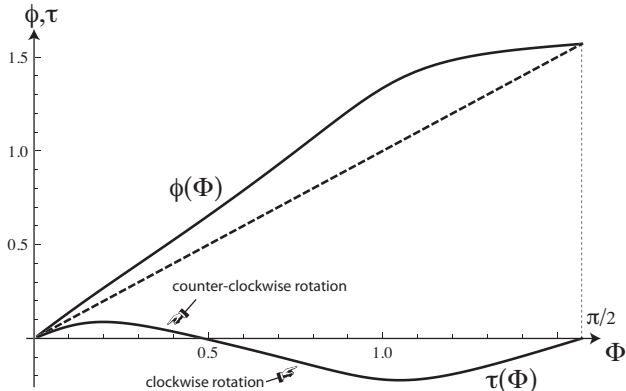


FIG. 3: Fiber orientation, ϕ , in the current configuration as a function of Φ , and the corresponding plot of $\tau(\Phi)$ ($\mu = 5$, $\zeta = 1.4$, $\nu = 1.1$). The dashed diagonal line corresponds to $\phi = \Phi$.

pression for $T_{\theta z}$ it is possible to obtain a lower bound, τ_{\min} , and a lower upper bound, τ_{\max} , for the torsion in the limit of large anisotropy $\mu_4 \gg \mu_1$, namely

$$\tau_{\min} = -\sqrt{(\zeta^2 - \nu^2)}/\nu\zeta, \quad \tau_{\max} = \sqrt{\mu}(\nu - 1)\nu/\zeta. \quad (2)$$

where $\mu = \mu_4/\mu_1$. There is currently no available experimental data regarding the value of μ .

We have shown that a fiber-reinforced elastic tube with right-handed helical fibers can rotate clockwise or counter-clockwise depending on the initial angle, axial extension, and initial stress in the fiber. We use this key result to develop a model of growing phycomycetes in which new fibers are continuously laid down in an evolving growth zone at the top of the sporangiophore. Our key assumptions are: (i) new fibers are laid down stress-free along the direction of fibers in the current configuration; (ii) the growth zone extends linearly in time to

a size h within the first two hours. A crucial concept is that the current configuration at a given time step becomes the reference configuration for the next time step. The overall growth process can now be explained as follows. Consider a material point in the cell wall. Initially fibers are laid down at some small angle Φ_0 with $\nu_0 = 1$ at the top of the growth zone. The extension (due to the turgor pressure) and the rotation (due to the relaxation of the torsional stress) of the cylinder result in the fibers re-orienting to an angle ϕ_1 . As growth proceeds, the material point moves downward with respect to the top of the growth zone and new fibers at the same material point are laid down with angle $\Phi_1 = \phi_1$ and zero stress. This material point now has a mixture of fibers with angles Φ_0 and Φ_1 . The effective stress in the fibers in this new reference configuration (at this material point) is thus a combination of fibers with pre-compressions ν_0 and ν_1 . A continuous model of this process is given by

$$\frac{\partial \Phi}{\partial t} = \kappa_1(\phi - \Phi), \quad \frac{\partial \nu}{\partial t} = \kappa_2(\zeta - \nu) \sin \Phi. \quad (3)$$

where Φ, ϕ, ν, ζ are all evaluated at Z , the distance from the top of the sporangiophore of a material point in the reference configuration. Following the property of the angle $\phi = \phi(\Phi)$ given above, we have $\Phi(t) \rightarrow \pi/2$ and $\nu(t) \rightarrow \zeta$ as $t \rightarrow \infty$. The time constant $1/\kappa_1$ is fitted so that when a material point leaves the growth zone the associated fiber is oriented along the axis, *i.e.* $\Phi(1) \approx \pi/2$ and similarly $1/\kappa_2$ is fitted to match the time for rotational inversion. As an example of the dynamics generated by this system (coupled to the equations for ϕ and τ), we show in Fig. 4 the evolution of τ, Φ , and ν as a function of time.

Each time the tube extends and twists as an elastic response to the extensional and torsional stresses, there is an evolution of the reference configuration due to the deposition of new fibers and other wall building materials. The net result is a continuous remodeling of the cell wall leading to an irreversible growth of the tube. The rotation of a small disk of height ΔZ at point Z measured from the top of the growth zone with fiber angle Φ and pre-compression ν (in the reference configuration) is $\Delta\theta = \tau(\Phi(Z), \nu(Z))\Delta z = \tau\zeta\Delta Z$. Thus the total rotational velocity, ω , can be estimated as

$$\omega = t_r^{-1} \int_0^H \tau(\Phi(Z), \nu(Z))\zeta dZ, \quad (4)$$

where t_r is a characteristic timescale corresponding to the remodeling time of the reference configuration.

We can now use our model for the evolution of the fiber angle and the fiber pre-compression to compute the rotational dynamics of our growing cylinder. We assume that the growth zone extends linearly in time with a constant velocity v_z up to a length $h = H\zeta$ (corresponding to the end of Stage IVa). Then the length of the growth

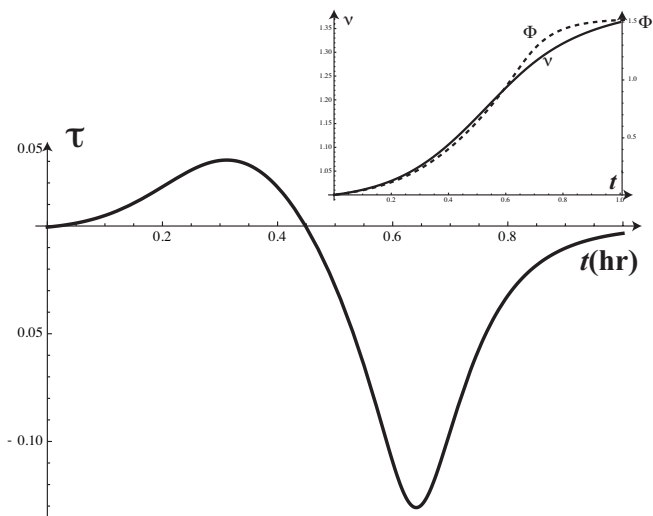


FIG. 4: Dynamic of τ , ν , and Φ for a given material point as a function of time ($\kappa_1 = 16\text{hr}^{-1}$, $\kappa_2 = 4\text{hr}^{-1}$, $\mu = 5$, $\zeta = 1.4$). While this process takes place, the material point at $t = 0$ starts on top of the growth zone and is convected downward (with respect to a reference frame moving with the top of the growth zone).

zone remains stationary (Stage IVb) and the tube extends, while rotating at a constant rate, until the growth zone retracts resulting in another inversion (Stage IVc). Fig 5 shows the results of such a simulation.

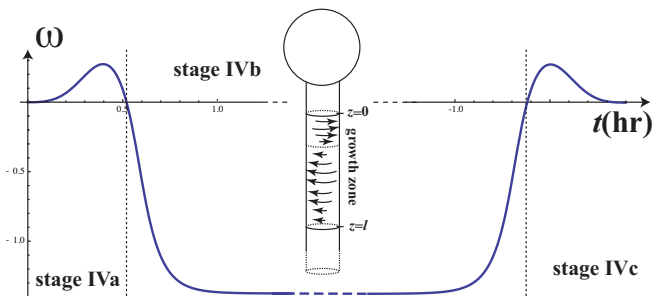


FIG. 5: Rotational velocity (in units of radians per unit time, t_r) of the sporangiophore as a function of time. The time -1 on the right-side of the time axis refers to one hour before the end of growth, *i.e.* the time in this simulation at which the growth zone starts to retract.

Initially before the growth zone is fully established, only the fibers in the top part of the zone play a role and the net rotation is counter-clockwise leading to right-handed growth (Stage IVa). Once the growth zone is fully established, the observed rotation of the sporangium is determined by the integral over the entire zone, hence leading to a left-handed spiral (Stage IVb). Interestingly, this model predicts that at any given time there are individual material points in the growth zone turning both counter-clockwise (top of the growth zone) and clockwise (bottom). The integrated effect of these rotations de-

pends on the extent of the growth zone. This is entirely consistent with the detailed observations of [13] on the rotation of individual points in the growth zone. Estimates of the rotational velocity depend on the choice of the time scale t_r . From Fig. 5 we see that in Stage IVb $|\omega| \sim 1.5$, and for the range of t_r , $1/\kappa_1 \leq t_r \leq 1/\kappa_2$, one finds the corresponding range of 1 to 4 turns/hr. This is qualitatively consistent with the observed 2 turns/hr.

The model proposed here for the rotational inversion of the sporangium in the aerial growth phase of phycomyces relies on two simple fundamental assumptions: first, new fibers are laid down along the direction of existing fibers; second, new fibers are laid down in a stress-free state. The rotational inversion is then a simple consequence of the mechanical response of a tubular, fiber-reinforced, morpho-elastic material, namely a material that responds elastically on short time scales (relieving torsional stress by rotation of the cylinder) and whose reference configuration evolves on longer time scales, leading to an irreversible (plastic-like) behavior. The beauty of the inversion phenomenon is that it relies on the non-linear anisotropic response of the system and leads to two apparent non-intuitive behaviors: first, the fibers tend to align with the axis, independently of the rotation; second, right-handed helical fibers can lead to both clockwise and counter-clockwise rotation depending on the angle and level of pre-compression.

Phycomyces are a simple but elegant example of the complex interplay between anisotropic response of fiber-reinforced biological materials and the effect of growth and remodelling. Many tissues and organs in plant and animal systems rely on similar mechanisms and a complete understanding of growing anisotropic material response is still lacking.

Acknowledgments: This publication is based in part upon work supported by the National Science Foundation under grant DMS-0907773 and by Award No. KUK-C1-013-04, made by King Abdullah University of Science and Technology (KAUST) (AG). AG is a Wolfson/Royal Society Merit Award holder.

-
- [1] J. B. Carnoy, Bull. Soc. Roy. Bot. Belgique **9**, 157 (1870).
 [2] R. Cohen and M. Delbrück, J. Gen. Physiol. **42**, 677 (1959). K. Bergman, P. Burke, E. Cerdá-Olmedo, C. David, M. Delbrück, K. Foster, E. Goodell, M. Heisenberg, G. Meissner, M. Zalokar, et al., Bacteriological Reviews **33**, 99 (1969). K. W. Foster and E. Lipson, J. Gen. Microbiol. **62**, 590 (1973). P. Galland, H. Finger, and Y. Wallacher, J. Plant Physiol. **161**, 733 (2004). P. Galland, Y. Wallacher, H. Finger, M. Hannappel, S. Tröster, E. Bold, and F. Grolig, Planta **214**, 931 (2002). D. Johnson and R. Gamow, J. Gen. Microbiol. **57**, 41 (1971). D. Johnson and R. Gamow, Plant Physiol. **49**, 898 (1972).

- [3] W. Astbury and R. Preston, Proc. Roy. Soc. London B **129**, 54 (1940). M. Middlebrook and R. Preston, Biochimica et biophysica acta **9**, 115 (1952). C. Lloyd and J. Chan, Plant Cell Online **14**, 2319 (2002). T. I. Baskin, Annu. Rev. Cell Dev. Biol. **21**, 203 (2005).
- [4] K. Schulgasser and A. Witztum, Wood Sc. and Tech. **41**, 133 (2007).
- [5] M. Middlebrook and R. Preston, Biochimica et biophysica acta **9**, 32 (1952). P. Roelofsen, Rec. Travaux Bot. Neerl. **42**, 72 (1950). P. Roelofsen and A. Houwink, Acta Bot. Neerl. **2**, 218 (1953).
- [6] E. Castle, Amer. J. Bot. **29**, 664 (1942).
- [7] P. Galland, E. Lipson, E. Cerdá-Olmedo, and E. Lipson, *Phycomyces* (Cold Spring Harbor Laboratory Cold Spring Harbor, NY, 1987). J. Ortega, G. Lesh-Laurie, M. Espinosa, E. Ortega, S. Manos, M. Cuning, and J. Olson, Planta **216**, 716 (2003).
- [8] J. Ortega and R. Gamow, J. Theor. Biol. **47**, 317 (1974). K. Yoshida, T. Ootaki, and J. Ortega, Planta **149**, 370 (1980). M. Wold and R. Gamow, Plant Physiol. **86**, 394 (1988).
- [9] M. Wold and R. Gamow, J. Theor. Biol. **159**, 39 (1992).
- [10] D. J. Cosgrove, J. K. E. Ortega, and W. Shropshire Jr, Biophys. J. **51**, 413 (1987).
- [11] P. Roelofsen, Adv. Bot. Res. **2**, 69 (1965).
- [12] J. Merodio and R. W. Ogden, Int. J. Solids Struct. **40**, 4707 (2003). H. Demirkoparan and T. J. Pence, J. Elasticity **92**, 61 (2008).
- [13] R. Cohen and M. Delbrück, J. Cell. Comparative Physiol. **52**, 361 (1958).

RECENT REPORTS

46/10	A theory for the alignment of cortical feature maps during development	Bressloff Oster
47/10	All-at-Once Solution of Time-Dependent PDE-Constrained Optimisation Problems	Stoll Wathen
48/10	Possible role of differential growth in airway wall remodeling in asthma	Moulton Goriely
49/10	Variational Data Assimilation Using Targetted Random Walks	Cotter Dashti Robinson Stuart
50/10	A model for the anisotropic response of fibrous soft tissues using six discrete fibre bundles	Flynn Rubin Nielsen
51/10	STOCHSIMGPU Parallel stochastic simulation for the Systems Biology Toolbox 2 for MATLAB	Klingbeil Erban Giles Maini
52/10	Order parameters in the Landau-de Gennes theory - the static and dynamic scenarios	Majumdar
53/10	Liquid Crystal Theory and Modelling Discussion Meeting	Majumdar Mottram
54/10	Modeling the growth of multicellular cancer spheroids in a bioengineered 3D microenvironment and their treatment with an anti-cancer drug	Loessner Flegg Byrne Hall Moroney Clements Hutmacher McElwain
55/10	Scalar Z, ZK, KZK, and KP equations for shear waves in incompressible solids	Destrade Goriely Saccomandi
56/10	The Influence of Bioreactor Geometry and the Mechanical Environment on Engineered Tissues	Osborne ODea Whiteley Byrne Waters
57/10	A numerical guide to the solution of the bidomain equations of cardiac electrophysiology	Pathmanathan Bernabeu Bordas Cooper Garny Pitt-Francis Whiteley Gavaghan
58/10	Particle-scale structure in frozen colloidal suspensions from small angle X-ray scattering	Spannuth Mochrie

60/10	Stochastic synchronization of neuronal populations with intrinsic and extrinsic noise	Bressloff Lai
61/10	Metastable states and quasicycles in a stochastic Wilson-Cowan model of neuronal population dynamics	Bressloff
62/10	Adsorption and desorption dynamics of citric acid anions in soil	Oburger Leitner Jones Zygalakis Schnepf Roose
63/10	A dual porosity model of nutrient uptake by root hairs soil	Zygalakis Kirk Jones Roose Wissuwa
64/10	Hot Charge Pairs and Charge Generation in Donor Acceptor Blends	Kirkpatrick
65/10	Excluded-volume effects in the diffusion of hard spheres	Bruna Chapman
66/10	Dynamics of colloidal particles in ice	Spannuth Mochrie Peppin Wettlaufer
01/11	Improving the efficiency of optical coherence tomography by using the non-ideal behaviour of a polarising beam splitter	Lippok Nielsen Vanholsbeeck
02/11	Self-diffusion in remodelling and growth	Epstein Goriely

Copies of these, and any other OCCAM reports can be obtained from:

**Oxford Centre for Collaborative Applied Mathematics
Mathematical Institute
24 - 29 St Giles'
Oxford
OX1 3LB
England
www.maths.ox.ac.uk/occam**